Volume 1 | Number 1 | Jan 2013 | Pages 1–100

Journal of
Materials Chemistry A

Materials for energy and sustainability
www.rsc.org/materialsA

ROYAL SOCIETY
OF CHEMISTRY

ROYAL SOCIETY
OF CHEMISTRY

www.rsc.org/materialsA

Journal Name

ARTICLE

Thermal conductivity of polymethylsilsesquioxane aerogels and xerogels with varied pore size for practical application to thermal superinsulators

G. Hayase,[a] K. Kugimiya,[b] M. Ogawa,[b] Y. Kodera,[a] K. Kanamori[a,*] and K. Nakanishi[a]

High-performance thermal insulating materials are desired especially from the viewpoint of saving energy for sustainable society. Aerogel is the long-awaited material for extended applications due to their excellent thermal insulating ability. These materials are, however, seriously fragile against even small mechanical stresses due to their low density, and the poor mechanical property has been inhibiting practical use as superinsulators. In this paper, we report relationships between thermal conductivity and pore and mechanical properties of organic-inorganic hybrid polymethylsilsesquioxane (PMSQ) aerogels with improved mechanical properties and controllable pore size from ~50 nm to 3 μm. Dependency of thermal conductivity on gas pressure and pore properties can be well explained by the thermal conduction theory of porous materials. These PMSQ aerogels show improved mechanical properties due to their elastic networks, which enable easier handling compared to conventional aerogels and facile production by simple ambient pressure drying. An aerogel-like "xerogel" monolithic panel has been successfully prepared via ambient pressure drying, and shows low thermal conductivity (0.015 W m^{-1} K^{-1}), which is comparable with the corresponding PMSQ aerogel and conventional silica aerogels. These results would open the gate for practical applications of these porous materials.

1   Introduction

It is no doubt that thermal insulation, which decreases the energy consumption in various processes, is one of the important issues today. Thermal insulating materials with low thermal conductivity are widely used in our life to keep desirable temperature in buildings, to protect from burns, and to reduce energy consumptions in electrical appliances such as refrigerators.[1] In industry, insulating materials are more extensively used for improving the energy balance in plants, preventing equipment from troubles, and transport and storage of liquefied gases. In addition, insulation of engines, batteries, and cargos in transportation is becoming increasingly crucial from the viewpoint of saving energy.

Aerogel is one of the most expected thermal insulating materials because of its lowest thermal conductivity among all solid materials.[2-5] Typical aerogels specially designed for the thermal insulating purpose show excellent insulation with thermal conductivity < 0.015 W m^{-1} K^{-1}, which is appreciably lower compared to those of classical insulating materials, 0.021–0.040 W m^{-1} K^{-1}.[2,3,6,7] Although commercially available vacuum insulation systems outstrip the insulation of aerogels,[8-10] the vacuum gradually degrades during long-term use by leak. Vacuum insulation therefore needs robust frameworks and might need regular maintenance to keep the high insulation. Aerogels, on the other hand, are stable solid as far as being hydrophobized,[11] and can be used at ambient pressure for long period of time. In addition, aerogel-based thermal insulation has a large advantage in saving space and weight for many applications including space development, because the less amount of insulating materials is required to achieve the comparable insulation to the traditional materials.[5,6,11] Especially in typical silica aerogels, aerogel glazing is expected as a transparent window superinsulating system,[5,6,12] because silica aerogels possess visible-light transmittance and low refractive index.[3] However, mechanical strength of these low-density materials is so low that they are easily cracked and collapsed even by a slight curvature caused during processing and by the wind while in use. Even worse is the requirement of a high-pressure supercritical fluid such as carbon dioxide (above 31°C and 7.37 MPa)[13] as the drying solvent to keep their porous structure throughout the drying process. Hence, there is a size limitation to monolithic aerogels because of the size of autoclaves that can be safely operated from technical and legal aspects. For this reason,

there has been limited precedent of large-area monolithic aerogels with, for example, the size of a window glass. Instead, aerogel granules and composites are widely employed for larger-area daylighting and wall insulation systems.[4,5]

To improve the mechanical properties of transparent aerogels, many researchers have been working on various strategies. One of the promising ways is organic-inorganic hybridization. For instance, Leventis and coworkers have been investigating several types of silica aerogel-polymer composite materials.[14-17] Although they succeeded in obtaining flexible aerogels durable against bending stress by laminating silica skeletons with organic polymers, their thermal conductivity is higher than pure silica aerogels due to the partial loss of mesoporosity. Our group has been studying on organic-inorganic hybrid aerogels whose crosslinked structure consists of organo-modified siloxane networks.[18-23] Polymethylsilsesquioxane (PMSQ, $CH_3SiO_{1.5}$) aerogels containing dangling methyl groups as the organic moiety show high strength and flexibility against compression. The compressive elasticity allows fabrication of aerogel-like "xerogels" through the "spring-back" behavior during drying at an ambient condition.[24,25] Their visible-light transmittance is almost the same with that of silica aerogels, and can be handled much easier due to their improved mechanical property, which is nonetheless still far from common thermal insulators such as glass wools, porous ceramic boards and organic polymer foams.

More recently, we succeeded to synthesize transparent and opaque PMSQ aerogels with continuously controlled pore size from 50 nm to 3 μm with nonionic surfactant Pluronic F127.[21] Although these aerogels are designed to possess rather high density (> 0.2 g cm^{-3}) in order to obtain co-continuous macroporous structure, mechanical properties such as Young's modulus are higher compared to the previous PMSQ aerogels, which enables even easier handling. In this paper, relationships between pore size, mechanical property and thermal conductivity with varied gas pressure are discussed with the PMSQ aerogels prepared with F127. Although several researchers reported the effects of pore size and gas pressure on thermal conductivity using carbon and silica aerogels in these 20 years,[26-31] this is the first report on the organic-inorganic hybrid aerogels with well-defined morphology and extensively variable pore size. We also demonstrate the possibility of PMSQ aerogel-like xerogels obtained by a simple drying process in ambient pressure and temperature as a practical insulating material with sufficiently low thermal conductivity of 0.015 W m^{-1} K^{-1}.

2 Experimental

2.1 Reagents

Acetic acid, methanol, 2-propanol and n-heptane were purchased from Kishida Chemical Ltd. (Japan). Distilled water and urea were from Hayashi Pure Chemical Ind., Ltd.

(Japan). Surfactant poly(ethylene oxide)-block-poly(propylene oxide)-block-poly (ethylene oxide) ($EO_{106}PO_{70}EO_{106}$, Pluronic F127, $M_w \sim 12600$) was from BASF (Germany). Methyltrimethoxysilane (MTMS) was obtained from Shin-Etsu Chemical Co., Ltd. (Japan). All reagents were used as received.

2.2 Synthesis procedure

The starting compositions are listed in Table 1. In a typical synthesis, 60 mL of diluted aqueous acetic acid (5 mM), 5 g of urea, and 0–10.0 g of surfactant (Pluronic F127) were mixed in a glass sample tube, and 50 mL of MTMS was subsequently added under vigorous stirring. Molar ratio of the starting materials is MTMS:water:acetic acid:urea:F127 = 1:9.6:0.00086:0.24:0–0.0023. After the mixed solution was continuously stirred for 30 min at room temperature to allow acid-catalyzed hydrolysis of MTMS, the resultant homogeneous solution was allowed to gel at 60 °C in a closed vessel. At this stage, urea hydrolyzes into ammonia, which promotes the base-catalyzed polycondensation of hydrolyzed MTMS.[32] Gelation time was 6–6.5 h for all samples, and phase separation (if induced) and gelation were almost concurrent. The wet gel was then aged for 4 d to complete the condensation, followed by washing with methanol for three times (more than 8 h at 60 °C for each time) to remove the surfactant, unreacted species, etc. The washed sample was subjected to solvent exchange with 2-propanol for three times in the identical way to washing. To dry the wet gels, supercritical drying and evaporative drying at ambient pressure and temperature were performed. For supercritical drying to obtain "aerogels", 2-propanol in wet gels was exchanged with supercritical carbon dioxide at 80 °C and 14 MPa in a custom-built autoclave (Mitsubishi Materials Techno Corp., Japan) followed by a slow depressurizing to atmospheric pressure. For evaporative drying to obtain "xerogels", wet gels were subjected to solvent exchange with n-heptane for three times, and heptane was slowly removed by evaporation at room temperature for ~ 1 d. Obtained xerogels were finally heated with a hot oven at 110 °C in air for 3 h to completely remove heptane and liberate remnant stress and shrinkage of the networks.

2.3 Measurements

Bulk density ρ was obtained from the weight/volume ratio of specimens. Porosity Φ was then determined as $\Phi = 1 - \rho/\rho_s$, where ρ_s represents skeletal density of the PMSQ network (1.40 g cm^{-3}) determined by helium pycnometry.[33] A scanning electron microscope (JSM-6700F, JEOL, Japan) was employed to observe the microstructure. Mechanical properties of aerogels were investigated with a material tester (EZGraph, Shimadzu Corp. (Japan)). For uniaxial compression tests, specimens carved from large panels (typical length × width × height is 15 × 15 × 10 mm^3) were compressed-decompressed using a load cell of 5 kN with a rate of 0.5 mm min^{-1}. For 3-point bending tests, carved

cuboid specimens were put on a fixture with a 15 mm span and loaded by a wedge-shaped crosshead with 60 ° tip and 0.3 mm diameter with using a load cell of 5 N at a rate of 1 mm min^{-1} to the point of brittle failure. Young's modulus E was calculated using the slope of linear region in stress-train curves between 0.1 and 0.2 MPa stress. For light

transmittance measurements, a UV−VIS spectrometer V-670 (JASCO Corp., Japan) equipped with an integrating sphere ISN-723 was employed. Direct-hemispherical transmittance was recorded, and obtained transmittance data at 550 nm were normalized into those corresponding to equivalent

Table 1 Starting compositions and properties of aerogels obtained in the present study.

| Materials	MTMS/mL	HOAc aq./mL	Urea/g	F127/g	E/MPa	T/%	ρ/g cm^{-3}	Φ
S3.2	50.0	60.0	10.0	3.20	27	0	0.45	0.68
S3.4	50.0	60.0	10.0	3.40	13	0	0.45	0.68
S3.6	50.0	60.0	10.0	3.60	14	0	0.41	0.70
S4.0	50.0	60.0	10.0	4.00	19	0	0.36	0.75
S6.0	50.0	60.0	10.0	6.00	17	2	0.29	0.80
S10.0	50.0	60.0	10.0	10.0	7	47	0.27	0.81

thickness of 10 mm using the Lambert−Beer equation. The normalized total transmittance is denoted as T. Thermal conductivity was measured under varied pressure on aerogels and under ambient pressure on aerogels/xerogels with a guarded hot plate system GHP 456 Titan and a transient heat flow meter HFM 436 Lambda (Netzsch GmbH (Germany)), respectively. The size of the specimens was $100 \times 100 \times 10$ mm^3. The values obtained in each measurement are roughly within the error of 5 %.

3   Results and discussion

3.1   Structure, mechanical properties and visible-light transmittance of obtained aerogels

Six aerogel panels were prepared via supercritical drying as shown in Table 1. The sample name Sx means an aerogel panel prepared with x g of F127 via supercritical drying. With increasing only the amount of surfactant F127 in the starting composition, the pore structure and properties are easily controlled as we reported previously.[21] Along with the variation in the microstructure, however, mechanical properties do not show a straightforward trend. This can be explained by the elaborate morphological change in the microstructure (Fig. 1). The sample S3.2 prepared with the least amount of F127 possesses well-defined continuous macropores derived from the transient structure of spinodal decomposition, the structure of which was "frozen" by the concurrent sol-gel transition.[34-40] The macropore skeletons contain a small amount of mesopores, and Young's modulus is the highest among all the aerogels prepared in this study (Table 1). With increasing F127 (x), the amount of mesopores inside the macropore skeletons of bicontinuous structure increases.[21] Samples S3.4 and S3.6 have thinner macropore skeletons and the fraction of mesopores is increased, both of which are resulted from the transient structure at an earlier stage of spinodal decomposition. The SEM images of these two samples show the porous structure with diffusive interfaces. The finer and disordered hierarchical pore structures result in the lower Young's modulus and higher fragility. With further increasing x, only small macropores are

confirmed as interstices of the reticular PMSQ networks, which are derived from microphase separation. Young's modulus of the aerogel S4.0 is higher than those of samples with the hierarchical pore structures, and the modulus decreases with a further increase of F127 in the starting composition, due to the finer structures derived from more effective suppression of phase separation. From these reasons, the S10.0 panel with ~15 nm skeletons[20] shows the lowest Young's modulus among the 6 samples. In fact, Young's modulus obtained from uniaxial compression and bending strength from 3-point bending are higher in these samples compared to the PMSQ aerogels synthesized with n-hexadecyltrimethylammonium chloride (CTAC) as reported previously,[22] due to the lower porosity and thicker and more continuous skeletons (Fig. S1, ESI†). The higher mechanical property in the present samples enables easier handling of the large panels.
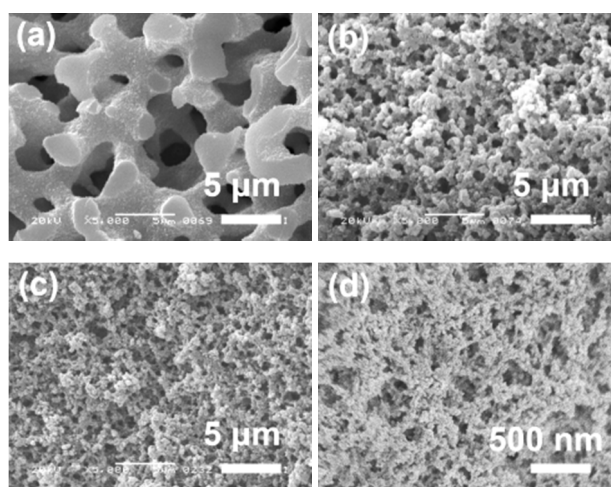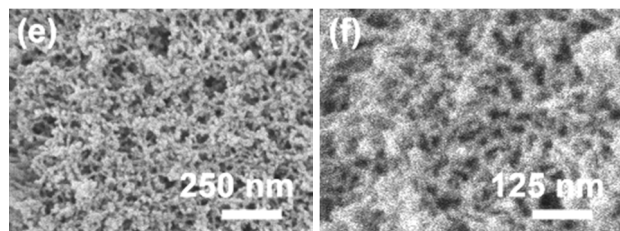
Fig. 1 SEM images of the aerogel samples. (a) S3.2, (b) S3.4, (c) S3.6, (d) S4.0, (e) S6.0 and (f) S10.0. The pore structure becomes finer from several microns to ~50 nm with increasing amount of F127 in the starting composition.

As for the optical property, S6.0 and S10.0 show some visible-light transmittance (Table 1 and Fig. 2). At $x > 6.0$, the average size of the pore structure decreases to < 100 nm (Fig. 1), where the contribution of the Mie scattering mode becomes small. With increasing amount of F127, since the length scale of the pore structure becomes sufficiently shorter (~50 nm) than the wavelength of visible light, appearance of the aerogel samples turns from opaque to bluish translucent, because the Rayleigh scattering becomes the dominant light scattering mode. These mechanical and optical properties do not degrade by humidity and UV irradiation due to the hydrophobicity (Fig. S2, ESI†) and the stability of the silicone polymer network of PMSQ, respectively.
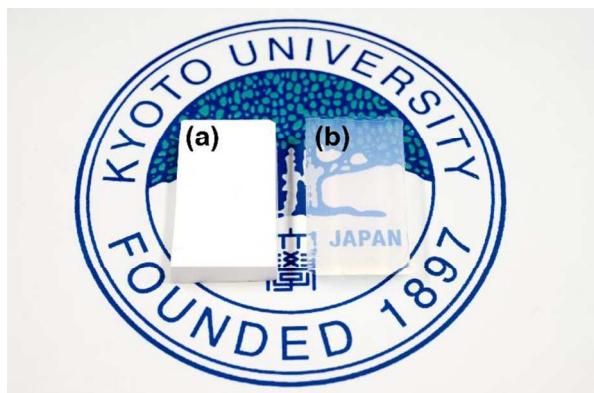

Fig. 2 Digital camera image of the obtained small aerogel samples; (a) S3.2 and (b) S10.0.

3.2 Relationship between gas pressure and thermal conductivity of aerogels

The total thermal conductivity λ_t of a porous material is the sum of three components; thermal conductivities of gas λ_g and solid λ_s, and by radiation λ_r.[26-29,31,40,41]

$$\lambda_t = \lambda_g + \lambda_s + \lambda_r \qquad (1)$$

The high thermal insulating ability of aerogels is mainly derived from the limited contributions from λ_g and λ_s. The suppression of λ_g can be explained by the relationship between pore size and the mean free path of gas molecules. Typical aerogels possess pore size shorter than the mean free path of the molecules in air, which is ~70 nm at ambient pressure. In this small space, thermal conduction by exchange of the kinetic energy of the molecules is strictly limited. In addition, since the solid fraction is low (~0.1), λ_s is also suppressed. In the conventional insulators such as expanded polymer foams, λ_g is much higher than that of aerogels because of the larger pore sizes (typically 10-1000 μm), although λ_s is sufficiently low because of the high porosity.

In detail, thermal conductivity of gas at given temperature can be theoretically calculated as proposed by Kaganer,[42]

$$\lambda_g = \Phi \frac{\lambda_{g,0}}{1 + 2\beta l p_0/[pD]} \qquad (2)$$

with Φ being porosity, p_0 reference gas pressure, p gas pressure, $\lambda_{g,0}$ thermal conductivity of the non-convectional free gas at p_0, β a constant including the interaction between the gas molecules and the pore walls, l the mean free pass of the gas molecules at p_0, and D average pore size of the porous material.

The total thermal conductivity of the present samples with varied pore size was measured under varied nitrogen gas pressure ranging from 10^2 to 10^5 Pa by the guarded hot plate (GHP) method, and the obtained experimental data were fitted with the theoretical curves by setting the parameters of p_0, $\lambda_{g,0}$ and β as 10^5 Pa, 0.026 W m^{-1} K^{-1} and 1.5, respectively (Fig. 3).[30,31]

$$\lambda_t = \frac{0.026}{1 + 21/pD} \Phi + \lambda_s + \lambda_r \qquad (3)$$

Porosity Φ of each sample is obtained and listed in Table 1. However, it is difficult to determine the average pore size D by porosimetry techniques such as mercury intrusion and nitrogen adsorption-desorption due to the flexibility of these PMSQ aerogels against compressive stress. Contributions of λ_s and λ_r also cannot be determined experimentally. Instead, we obtained D and $\lambda_s + \lambda_r$ (Table 2) from the fitting curves of each aerogel panel, and the obtained D of each sample agree with the SEM images (Fig. 1). In the cases of S3.2 and S3.4, deviations of experimental curves from the fitting curves are confirmed at the low-pressure region. These deviations are derived from an incomplete contact between the plates of the device and the slightly warped aerogel surface. Other parts of the data show a good agreement between experimental and theoretical curves. Thermal conductivity of these PMSQ aerogels can therefore be explained and anticipated from the theory of thermal conductivity of porous materials.
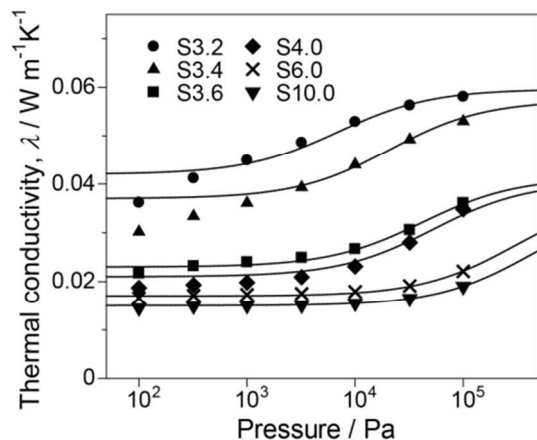
Fig. 3 Relationship between thermal conductivity and gas pressure on PMSQ aerogel samples with different pore sizes. The solid lines are calculated from the theoretical consideration.

Table 2 Average pore size D and the sum of solid and radiative thermal conductivities $\lambda_s + \lambda_r$ of the aerogel samples obtained by fitting results.

Materials	D/m	$(\lambda_s + \lambda_r)$/W m^{-1} K^{-1}
S3.2	3×10^{-6}	0.042
S3.4	1×10^{-6}	0.037
S3.6	5×10^{-7}	0.023
S4.0	4×10^{-7}	0.021
S6.0	7×10^{-8}	0.017
S10.0	5×10^{-8}	0.015

To design better insulating aerogels, there are two major strategies; decreasing λ_g or $\lambda_s + \lambda_r$. In this system, λ_g can be made lower when the amount of F127, x, in the starting composition is increased, predominantly due to the decreased average pore size by the enhanced suppression of phase separation during gelation. At the same time, it is clear from Fig. 3 that even a light evacuation like 10^4 Pa can effectively reduce thermal conductivity to 0.015−0.025 W m^{-1} K^{-1} except for the samples with relatively large macropores (S3.2 and S3.4). This is highly advantageous for the design of high-performance insulators, because these insulating samples show higher mechanical strength compared to the conventional aerogels and accordingly higher facility of obtaining crack-free panels by ambient pressure drying. On the other hand, the sum of solid and radiative conductivities, $\lambda_s + \lambda_r$, becomes lower with increasing x in the starting composition, mostly due to lower solid conductivity of the lower-density samples. To further reduce $\lambda_s + \lambda_r$, density of the aerogels should be decreased by changing the starting composition by, for instance, decreasing the concentration of MTMS. By this way, however, the controllability of pore size decreases due to lower gel formation ability and higher phase separation tendency in the diluted sols. Overall, in the present system, S10.0 is the best insulator among the 6 samples, because both λ_g and $\lambda_s + \lambda_r$ is reduced. In addition, this sample shows the highest visible-light transmittance T as mentioned

above. In the next section, a preparation of an S10.0 xerogel insulating panel is demonstrated as a candidate of practical superinsulators.

3.3 Preparation of highly-insulating aerogel-like xerogels

Recent years, we have reported PMSQ aerogel-like xerogels with almost the same properties as corresponding PMSQ aerogels, without relying on supercritical drying.[18,19] Although low-density (~0.14 g cm^{-3}) and highly transparent (~90 % at 550 nm) aerogel-like xerogels can be obtained with cationic surfactant like CTAC and its bromide counterpart CTAB, it is still difficult to prepare large-area xerogel panels for practical insulating applications due to relatively high fragility. Since aerogels prepared under the co-presence of F127 are mechanically more robust than those prepared with other surfactants (Fig. S1, showing higher bending strength), there is a high possibility to easily obtain crack-free large-area panels via ambient pressure drying. Using F127 as the surfactant, this is the first report on the preparation of an aerogel-like xerogel panel, and their thermal insulating ability was evaluated. To successfully obtain PMSQ aerogel-like xerogels, the most important loadstar of the gel is elasticity enough to recover their original size and shape from 50 % uniaxial compression, because wet gels undergo *ca.* 50 % of linear shrinkage by capillary force in the pores. Among the samples discussed above, S10.0 shows the highest recovery performance from uniaxial strain (Fig. 4) in addition to the highest insulating ability and transparency. We therefore attempted to obtain a S10.0 xerogel panel by ambient pressure drying.
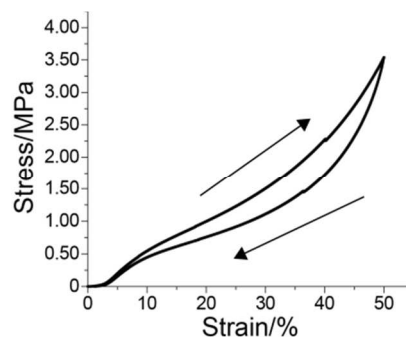

Fig. 4 Stress-strain curve of S10.0 obtained by uniaxial compression-decompression.

We first tested drying of small wet gels with a disk-shape of *ca.* 5 mm height and 10 mm diameter. As a result, obtained aerogel-like xerogels had almost the same density as S10.0 aerogels; however, all the samples suffered from small cracks (see Movie S1, ESI†). In the case of large wet gel panels, the drying gels started cracking at the early stage of drying, and finally were broken into several pieces. This is because the S10.0 wet gel is too rigid and less bendable, and is fragile against the high stress (estimated as >1.5 MPa) during the drying process. To increase the flexibility, gels with lower

density were prepared by increasing the amount of aqueous acetic acid in the starting composition. By using more than 80 mL (cf. 60 mL in the original composition) of aqueous acetic acid (and proportionally, 6.7 g of urea), crack-free aerogel-like xerogel samples were successfully obtained by ambient pressure drying. The progress of drying is captured as a movie and shown in Movie S2, ESI†: after evaporation of the bulk drying solvent n-heptane, the gel starts shrinking by the capillary force exerted on the outer surface of the gel. At the critical point (the leatherhard point),[43] the gel suddenly turns into opaque due to the critical opalescence, and then the gel undergoes spring-back as relaxation of the capillary force on emptying the pores. The obtained panel synthesized with 80 mL of aqueous acetic acid (named A10.0, shaped in $100 \times 100 \times 10$ mm^3) possesses aerogel-like properties and microstructures (Fig. 5 and Table S1, ESI†), and shows sufficiently low thermal conductivity of 0.015 W m^{-1} K^{-1}, which is even lower than that of S10.0 due to the decreased density and $\lambda_s + \lambda_r$. The xerogel panel exhibits certain transparency (29 %), whereas it is lower than the PMSQ aerogels and xerogels obtained by using CTAB/CTAC as surfactant (~90 %). The present example of a monolithic aerogel-like xerogel with visible-light transmittance and low thermal conductivity would be the first step to bring up the transparent airy materials to a practical large-area insulator that would be used extensively.
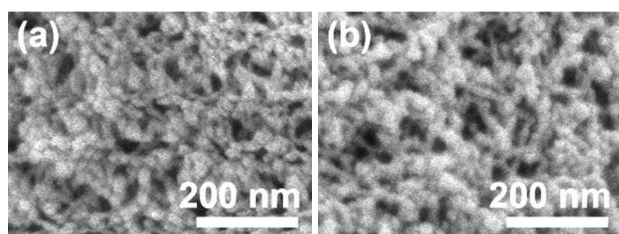

Fig. 5 SEM images of A10.0 obtained via (a) ambient pressure drying and (b) supercritical drying.

Conclusions

Large-area panels of organic-inorganic hybrid PMSQ aerogel with uniform meso- and macropores have been prepared. Pore size has been widely controlled from ~50 nm to 3 μm simply by changing the amount of nonionic surfactant F127 in the starting composition. Thermal conductivity of each aerogel sample varies depending on the gas pressure, and shows a good agreement with the theoretical values. Aerogel panels with larger average pore size trend toward higher thermal conductivity, which can be effectively decreased by lightly reducing the gas pressure; $e.g.$ to 10^4 Pa. Aerogel samples with small pores already exhibit low thermal conductivity (0.015–0.020 W m^{-1} K^{-1}) at ambient pressure, which shows these aerogels can be used as a highly insulating material under ambient or lightly reduced pressure. This is advantageous when considering conventional vacuum insulation requires highly conductive robust frameworks and regular maintenance to keep the performance. An aerogel-like xerogel panel with sufficiently low thermal conductivity (0.015 W m^{-1} K^{-1}) and visible-light transmittance (29 % through 10 mm thickness at 550 nm) has also been prepared. Through further improvement of these materials, a new daylighting/transparent thermal insulating system would be developed for practical utilizations in the near future.

Notes and references

[a] Department of Chemistry, Graduate School of Science, Kyoto University, Kitashirakawa, Sakyo-ku, Kyoto 606-8502, Japan.

[b] Japan Fine Ceramics Center, 2-4-1 Mutsuno, Atsuta-ku, Nagoya 456-8587, Japan.

† Electronic Supplementary Information (ESI) available: movies of ambient pressure drying and some additional properties of the prepared aerogels/xerogels. See DOI: 10.1039/b000000x/

1. B. P. Jelle, *Energ. Buildings*, 2011, **43**, 2549-2563.
2. J. Fricke and T. Tillotson, *Thin Solid Films*, 1997, **297**, 212-223.
3. N. Hüsing and U. Schubert, *Angew. Chem. Int. Ed.*, 1998, **37**, 23-45.
4. M. Koebel, A. Rigacci, P. Achard, *J. Sol-Gel Sci. Technol.*, 2012, **63**, 315-339.
5. M. A. Aegerter, N. Leventis and M. M. Koebel, in *Aerogels Handbook*, Springer, New York, 2011, pp. 607-633.
6. L. W. Hrubesh and R. W. Pekala, *J. Mater. Res.*, 1994, **9**, 731-738.
7. L. W. Hrubesh, *J. Non-Cryst. Solids*, 1998, **225**, 335-342.
8. S. Brunner and H. Simmler, *Vacuum*, 2008, **82**, 700-707.
9. R. Baetens, B. P. Jelle, J. V. Thue, M. J. Tenpierik, S. Grynning, S. Uvslokk and A. Gustavsen, *Energ. Buildings*, 2010, **42**, 147-172.
10. S. Brunner and K. G. Wakili, *Vacuum*, 2014, **100**, 4-6.
11. J. P. Randall, M. A. B. Meador and S. C. Jana, *ACS Appl. Mater. Interfaces*, 2011, **3**, 613-626.
12. K. I. Jensen, J. M. Schultz, F. H. Kristiansen, *J. Non-Cryst. Solids*, 2004, **350**, 351-357.
13. A. C. Pierre and G. M. Pajonk, *Chem. Rev.*, 2002, **102**, 4243-4265.
14. G. Zhang, A. Dass, A.-M. M. Rawashdeh, J. Thomas, J. A. Counsil, C. Sotiriou-Leventis, E. F. Fabrizio, F. Ilhan, P. Vassilaras, D. A. Scheiman, L. McCorkle, A. Palczer, J. C. Johnston, M. A. Meador and N. Leventis, *J. Non-Cryst. Solids*, 2004, **350**, 152-164.
15. M. A. B. Meador, E. F. Fabrizio, F. Ilhan, A. Dass, G. Zhang, P. Vassilaras, J. C. Johnston and N. Leventis, *Chem. Mater.*, 2005, **17**, 1085-1098.
16. U. F. Ilhan, E. F. Fabrizio, L. McCorkle, D. A. Scheiman, A. Dass, A. Palczer, M. B. Meador, J. C. Johnston and N. Leventis, *J. Mater. Chem.*, 2006, **16**, 3046-3054.
17. N. Leventis, *Acc. Chem. Res.*, 2007, **40**, 874-884.

18. K. Kanamori, M. Aizawa, K. Nakanishi and T. Hanada, *Adv. Mater.*, 2007, **19**, 1589-1593.

19. K. Kanamori, M. Aizawa, K. Nakanishi and T. Hanada, *J. Sol-Gel Sci. Technol.*, 2008, **48**, 172-181.

20. K. Kanamori, K. Nakanishi and T. Hanada, *J. Ceram. Soc. Jpn.*, 2009, **117**, 1333-1338.

21. K. Kanamori, Y. Kodera, G. Hayase, K. Nakanishi and T. Hanada, *J. Colloid Interface Sci.*, 2011, **357**, 336-344.

22. G. Hayase, K. Kanamori and K. Nakanishi, *Microporous Mesoporous Mater.*, 2012, **158**, 247-252.

23. M. Kurahashi, K. Kanamori, K. Takeda, H. Kaji and K. Nakanishi, *RSC Adv.*, 2012, **2**, 7166-7173.

24. S. S. Prakash, C. J. Brinker and A. J. Hurd, *J. Non-Cryst. Solids*, 1995, **190**, 264-275.

25. S. S. Prakash, C. J. Brinker, A. J. Hurd and S. M. Rao, *Nature*, 1995, **374**, 439-443.

26. X. Lu, M. C. Arduinischuster, J. Kuhn, O. Nilsson, J. Fricke and R. W. Pekala, *Science*, 1992, **255**, 971-972.

27. X. Lu, P. Wang, M. C. Arduinischuster, J. Kuhn, D. Buttner, O. Nilsson, U. Heinemann and J. Fricke, *J. Non-Cryst. Solids*, 1992, **145**, 207-210.

28. X. P. Lu, O. Nilsson, J. Fricke and R. W. Pekala, *J. Appl. Phys.*, 1993, **73**, 581-584.

29. X. Lu, R. Caps, J. Fricke, C. T. Alviso and R. W. Pekala, *J. Non-Cryst. Solids*, 1995, **188**, 226-234.

30. K. Swimm, G. Reichenauer, S. Vidi and H. P. Ebert, *Int. J. Thermophys.*, 2009, **30**, 1329-1342.

31. R. Baetens, B. P. Jelle and A. Gustavsen, *Energ. Buildings*, 2011, **43**, 761-769.

32. C. J. Brinker and G. W. Scherer, in *Sol-Gel Science: The Physics and Chemistry of Sol-Gel Processing*, Academic Press, San Diego, 1990, pp. 108-216.

33. L. J. Gibson and M. F. Ashby, in *Cellular Solids: Structure and Properties*, Cambridge University Press, Cambridge, 2nd edn., 1999, ch. 2.

34. K. Kanamori, H. Yonezawa, K. Nakanishi, K. Hirao and H. Jinnai, *J. Sep. Sci.*, 2004, **27**, 874-886.

35. K. Nakanishi and K. Kanamori, *J. Mater. Chem.*, 2005, **15**, 3776-3786.

36. H. Dong, M. A. Brook and J. D. Brennan, *Chem. Mater.*, 2005, **17**, 2807-2816.

37. K. Kanamori, K. Nakanishi and T. Hanada, *J. Sep. Sci.*, 2006, **29**, 2463-2470.

38. H. Dong and J. D. Brennan, *Chem. Mater.*, 2006, **18**, 4176-4182.

39. H. Dong and J. D. Brennan, *Chem. Mater.*, 2006, **18**, 541-546.

40. K. Kanamori and K. Nakanishi, *Chem. Soc. Rev.*, 2011, **40**, 754-770.

41. G. Wei, Y. Liu, X. Zhang, F. Yu and X. Du, *Int. J. Heat Mass Transfer*, 2011, **54**, 2355-2366.

42. M. G. Kaganer, in *Thermal Insulation in Cryogenic Engineering*, IPST Press, Jerusalem, 1969.

43. G. W. Scherer, *J. Am. Ceram. Soc.*, 1990, **73**, 3-14.

Journal of Materials Chemistry A Accepted Manuscript

For TOC

Relationship between thermal conductivity, gas pressure and pore size of polymethylsilsesquioxane aerogels and xerogels has been investigated for practical applications.